Quench propagation at different conditions in an HTS pancake coil wound with Roebel cable

Published Version:
Cavallucci, L., Breschi, M., Ribani, P.L., Pelegrin, J., Zhang, Q., Bailey, W., et al. (2021). Quench propagation at different conditions in an HTS pancake coil wound with Roebel cable. IEEE TRANSACTIONS ON APPLIED SUPERCONDUCTIVITY, 31(5), 1-5 [10.1109/TASC.2021.3070481].

Availability:
This version is available at: https://hdl.handle.net/11585/875277 since: 2024-07-04

Published:
DOI: http://doi.org/10.1109/TASC.2021.3070481

Quench Propagation at Different Conditions in a HTS Pancake Coil Wound with Roebel Cable

L. Cavallucci, M. Breschi, P. L. Ribani, J. Pelegrin, Q. Zhang, W. Bailey, Y. Yang

***Abstract*—The analysis of quench is of paramount importance for the safe operation of any superconducting magnet and this investigation is more relevant, even not fundamental, to prevent damage or burn-out in HTS magnets. Given these premises, quench tests and numerical models are indispensable. A $1\,\mathrm{D}$ electro-thermal model was developed at the University of Bologna (Italy) and validated versus experimental quench tests performed at the University of Southampton (UK) on a pancake coil wound with REBCO Roebel cable in the frame of the EUCARD-2 European Project. The analysis here presented investigates quench in the Roebel-based coil in case of a thermal disturbance introduced in the coil. The quench energies measured during tests as a function of the power disturbance are compared with the computed results. The quench energy is furthermore analysed energizing the coil at different transport current. The analysis is further extended to study the quench of the coil at temperatures of $66\,\mathrm{K}$ and at field of $2\,\mathrm{T}$.**

***Index Terms*—HTS, REBCO Roebel Cable, Pancake Coil, Quench, Modelling.**

I. Introduction

In the recent years, the scientific community is devoting great efforts to the applications of REBCO-based material to superconducting magnets [1], [2] and several cable configurations based on REBCO tapes are proposed in the literature [3], [4]. The ability of REBCO Roebel cables to carry high transport currents with a compact design and mechinical flexibility make them a promising technology in several applications, from high-energy physics [5], [6] to AC and DC power devices [7], [8]. Several studies have been published analysing the quench and AC losses in Roebel cables from both numerical [9] - [12] and experimental [13] - [17] point of view.

A $1\,\mathrm{D}$ electro-thermal model was proposed in [18] suitable for the study of quench in Roebel cables. The Roebel cable model proposed in [18] was extended in [19] to pass from the description of the cable itself to that of a Roebel-based pancake coil [20]. The model includes the description of heat transfer to the liquid nitrogen bath, the distributions of magnetic flux density and field angle relative to the tape over the coil, the epoxy impregnation and the thermal contact between coil turns at the strand level.

L. Cavallucci, M. Breschi and P.L. Ribani are with the Department of Electrical, Electronic, and Information Engineering, University of Bologna, 40136 Bologna, Italy (e-mail: lorenzo.cavallucci3@unibo.it; marco.breschi@unibo.it; pierluigi.ribani@unibo.it).

J. Pelegrin, Q. Zhan, W. Bailey and Y. Yang are with the Institute of Cryogenics, Faculty of Engineering and the Environment, University of Southampton, SO18 Southampton, United Kingdom (e-mail: Y.Yang@soton.ac.uk).

Manuscript received November 28, 2020; revised 2020.

In the present work, the model is applied to analyse quench at different transport currents and heater pulses. The computed results are compared here with measured quench energies. The model is further applied to investigate quench at working conditions of $66\,\mathrm{K}$ and $2\,\mathrm{T}$ background field. The impact of this working conditions on the current redistribution length and normal zone propagation velocity is presented. This condition was selected as a careful approach towards $4.2\,\mathrm{K}$ - $10\,\mathrm{T}$ condition that are under investigation.

II. Model Description

In the electro-thermal model, the strands of the Roebel cable are described with a $1\,\mathrm{D}$ FEM approach by the software COMSOL Multiphysics [21]. The model solves an array of $(2N+1)$ unknowns, where N is the number of strands of the Roebel cable. The unknowns are the temperatures of each strand (T_i), the temperature of the inter-turn insulation layer (T_{ins}) and the strand voltages (V_i).

A. Heat Balance Equations

A system of coupled heat balance equations is solved to determine the temperatures of all strands and the temperature of the insulation between turns:

$$\rho\, C_p(T_i))\ \frac{\partial T_i(x,t)}{\partial t} - \frac{\partial}{\partial x}\left(k(T_i)\ \frac{\partial T_i(x,t)}{\partial x}\right) =$$
$$+\sum_j^N f_{i,j}(x)\frac{T_i(x,t)-T_j(x,t)}{R^c_{th}\ \delta} + f_i^{\text{out}}(x)\ \frac{T_i(x,t)-T_{\text{ins}}\,(x',t)}{R^c_{th,\text{ins}}\,(T_{\text{ins}})\ \delta}+$$
$$+ f_i^{\text{in}}(x)\ \frac{T_i(x,t)-T_{\text{ins}}\,(x',t)}{R^c_{th,\text{ins}}\,(T_{\text{ins}})\ \delta} + Q_i^{\text{Joule, L}}(x,t)$$
$$+\sum_j^N Q_{i,j}^{\text{Joule, T}}(x,t) + Q_i^{\text{heater}}(x,t) + Q_i^{\text{LN}}(x,t) \qquad (1)$$

where $T_i(x)$ is the temperature of the *i*-th strands as a function of the longitudinal direction x, ρ the homogenized density, $C_p(T_i)$ the homogenized specific heat, $k(T_i)$ the longitudinal thermal conductivity, T_{ins} the temperature of the inter-turn insulation layer and δ the thickness of the strand.

The parameter R^c_{th} is the distributed thermal contact resistance per unit surface between strands in contact while $R^c_{th,\text{ins}}$ is the inter-turn thermal contact resistance.

In (1), the function $f_{i,j}(x)$ describes the local contact area between the *i*-th and the *j*-th strand; its values are included between 0 and 1. The function is equal to 1 at the regions of overlapping between the two strands, while it is null where the two strands are not in contact. A similar definition applies for the functions $f_i^{\text{out}}(x)$ and $f_i^{\text{in}}(x)$ that describe the contact between the *i*-th strand and the insulation at the outer and at the inner turns respectively [19].

The terms $Q_i^{\text{Joule, L}}$ and $Q_{i,j}^{\text{Joule, T}}$ take into account the joule power in the coil due to currents flowing respectively in the longitudinal and radial directions. The term Q_i^{LN} takes into account the heat exchange towards the liquid nitrogen bath [22], [23]. At operating temperatures lower than 77 K, the coil is assumed adiabatic and Q_i^{LN} is set to zero.

As for the boundary conditions, the temperature is kept fixed at the terminals of the coil, at the value corresponding to the initial operating temperature.

B. Current Density Continuity Condition

The model is able to solve the continuity of current density for the *i*-th strand accounting for the contributions along the longitudinal (x) and across the transverse (y) directions:

$$\frac{\partial}{\partial x}\left(-\sigma_i\left(T_i, E_i, B_i\right)\frac{\partial V_i(x,t)}{\partial x}\right) = \sum_j f_{i,j}(x)\ \sigma_{el}^c\ \frac{V_j(x,t)-V_i(x,t)}{\delta} \qquad (2)$$

where $\sigma_i\left(T_i(x,t), E_i(x,t), B_i(x,t)\right)$ is the homogenized longitudinal electrical conductivity as a function of temperature, electric field and magnetic flux density and σ_{el}^c is the electrical contact conductance between strands in contact.

As a boundary conditions, an equipotential surface is imposed on both terminals of the coil. At the inner terminal, the current density is imposed for all strands in order to set the total operation current.

C. Homogenization Procedure

The superconducting tape is represented through a homogeneous material with uniform properties. The longitudinal electrical conductivity is computed as a function of the position, assuming all the layers of the tape to be connected in parallel [18], [24]. A non-linear power law is used as a constitutive electric characteristic of the superconducting layer, with the critical current expressed as a function of temperature, magnetic flux density, and field angle with respect to the tape surface. The critical surface is described through the parametrization developed in [25].

III. Validation and Results

A piece of $2\,\text{m}$ long Roebel cable made of 15 strands of punched $2\,\text{G}$ YBCO tapes fabricated by Bruker EST was wound into a 7-turn pancake coil, shown in Fig. 1. The cable, with a transposition pitch of 226 mm, was assembled at Karlsruhe Institute of Technology (KIT, Germany). A length of 200 µm thick fiberglass ribbon was co-wound as the electrical insulation layer and to prevent delamination due to mismatch of the thermal expansion coefficient between the epoxy and the YBCO strand. The coil was further impregnated with epoxy resin. At the 4-th turn of the coil, a miniature heater (33 Ω) was attached to a copper-shim directly in contact with strand #7 at the inner face of the turn (between turns #4 and #3). During tests, the heater is fired to induce quench in the coil. The main geometrical parameters of the Roebel cable and pancake coil are collected in Table I.

TABLE I: Main Parameters of the Roebel-based Pancake Coil.

Roebel Cable	
transposition pitch T_p	226 mm
strands number	15
inter-strand electrical conductance σ_{el}^c	2.0×10^7 S/m^2
inter-strand thermal resistance R_{th}^c	7.0×10^{-4} K m^2/W 7.0×10^{-3} K m^2/W (heater)
Pancake Coil	
turns number	7
inner radius	72 mm
inter-strand insulation layer δ_{ins}	200 µm
top pancake insulation layer $\delta_{ins,s}$	500 µm

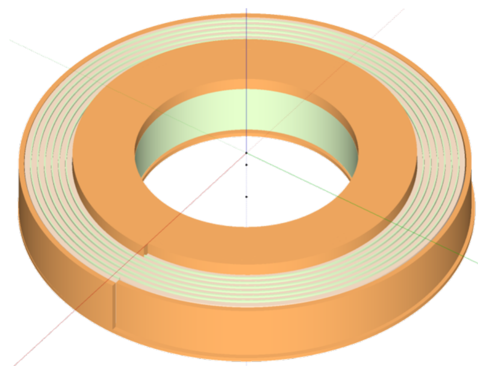

Fig. 1: Scketch of the Roebel-based pancake coil.

For each strand, a voltage-tap pair (Vna and Vnb) separated by one pitch length was soldered on either side of the heater. The voltage difference ΔVn is measured during tests as:

$$\Delta Vn = Vna - Vnb \qquad n = 1, \ldots, 15 \qquad (3)$$

As for the working conditions at 77 K, the coil is cooled through immersion in liquid nitrogen bath. To achieve lower temperatures, helium vapour at controlled mass rate and temperature (5 K - 100 K) flows through the coil and the terminal current leads. Further details about the experimental set-up are presented in [20].

A. Impact of Heater Power on Quench

As for the working conditions at 77 K, self field and 400 A transport current, the quench energies are investigated as a function of the power introduced by the heater. In Fig. 2, the quench energies measured during tests are compared with the numerical results. For heater power above 0.48 W, a difference below 10 % is found between experiments and computations while at 0.44 W a higher mismatch is found, still below 20 %. Figure 2 also reports the maximum temperature difference during quench, i.e. the hot spot temperature with respect to the reference temperature (77 K).

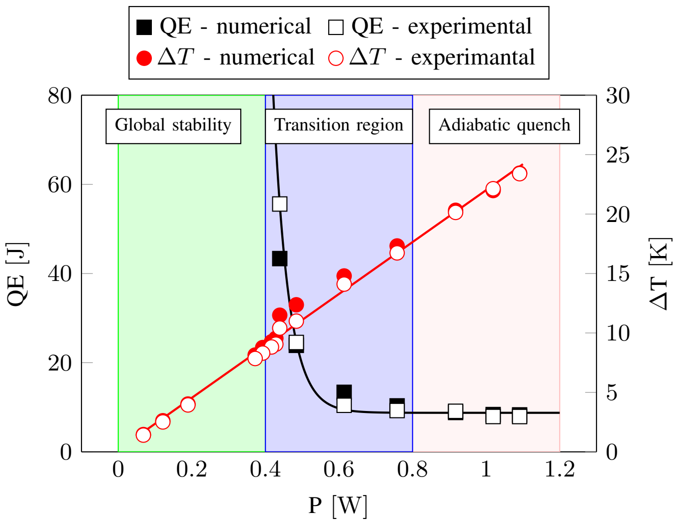

Fig. 2: Quench energies as a function of heater power at 77 K, self field and 400 A transport current. On the right axes, the difference of the hot sport temperature with respect to the reference temperature is shown.

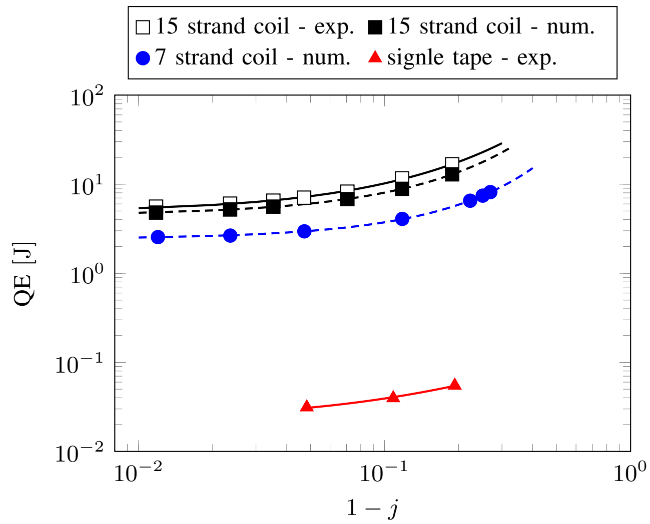

Fig. 3: Quench energies as a function of transport current at 77 K, self field and heater pulse of 1.0 W.

For heater power levels above 0.8 W, the quench energy is not significantly affected by power and it is stable about 8 J - 9 J. Instead, for power values between 0.4 W and 0.8 W, the quench energy is significantly affected by the heater power. The lower is the heater power, the longer is the heater pulse necessary to quench the coil. For heater powers below 0.4 W, even longer heater pulses are not able to quench the coil. In this case, heat and currents redistribute between strands without any transition to the normal state.

B. Impact of Transport Current on QE

The quench energies were measured at different values of transport current. In these tests the coil is in self-field cooled by liquid nitrogen bath and the heater power is about 1.0 W. The experimental results are compared in Fig. 3 with the computed quench energies. The energies are shown as a function $(1-j)$ where j is the ratio between the transport current and the measured critical current ($I_c \sim 465$ A).

The coil wound with the 15-strand cable exhibits a quench energy of about 5 J for a current of 444 A, corresponding to about 99% of the critical current and 13 J at 365 A, 80 % of the critical current. The model is further applied to investigate the impact of the number of strand in the cable. In Fig. 3, the energies are computed for a coil assembled with a 7-strand cable. In this case, the quench energies are about 50 % lower than for the coil wound with the 15-strand cable. The quench energies measured on an individual REBCO tape in [26] are also added in Fig. 3. The individual tape exhibits quench energies up to 200 times lower than the coil.

C. Quench at 66 K and 2 T background field

In the working conditions at 66 K, 2 T background field and transport current of 700 A ($I_c \sim 750$ A), the quench is initiated by firing the heater for 6.5 s, for a total amount of 6.5 J. The voltages measured during quench are compared in Fig. 4 with the numerical results. The voltages exhibit a peak of about 1.5 mV for strand #7 and a peak below 0.5 mV for strands #2 and #15. The maximum difference between experimental and numerical results is found for the signal $\Delta V7_0$. It is worth of noting that this signal is acquired near the heater and so it is more affected by uncertainty.

Figure 5 shows the computed transverse current flowing between strands #7-#6, #5-#6, #7-#8 and #8-#9 at $t = 7.5$ s. At $t = 7.5$ s, strand #7 is normal conducting and the current flows from #7 towards the neighbouring strands, so that the current on strand #7 reaches a minimum. The transverse currents exhibit a peak of about $12.0\,\mathrm{kA\,m^{-2}}$ between strands #7-#6 and #7-#8, i.e. the strands directly in contact with the strand #7. The transverse current is lower for strands #5-#6 and #8-#9. For all strands, the current redistributes along the whole coil, instead in the working conditions at 77 K and self-field [19] the current redistribution occurs over half of the coil mainly before the heater.

D. Normal Zone Propagation Velocity

The normal zone propagation velocity (NZPV) is computed analysing the voltage differences ΔVn derived from the model. A reference time instant t_n^* is selected as the instant when the evolution in time of ΔVn overcomes the threshold Vn_c. The NZPV is consequently computed for each strand as;

$$\mathrm{NZPV}_n = \frac{L_n}{t_n^*} \qquad n = 1,\ \ldots,\ 15 \tag{4}$$

where L_n is the distance between a pair of voltage tap, nominally equal to the cable twist pitch. The threshold Vn_c is defined as the voltage corresponding to 10 times the critical field E_c set to $10^{-4}\,\mathrm{V\,m^{-1}}$ [27], i.e.:

$$Vn_c = 10\,E_c\,L_n \approx 0.23\,\mathrm{mV} \tag{5}$$

In Fig. 6, the NZPV of strands #2, #4, #6, #8, #10, #12 and #14 is computed at different operating conditions. The

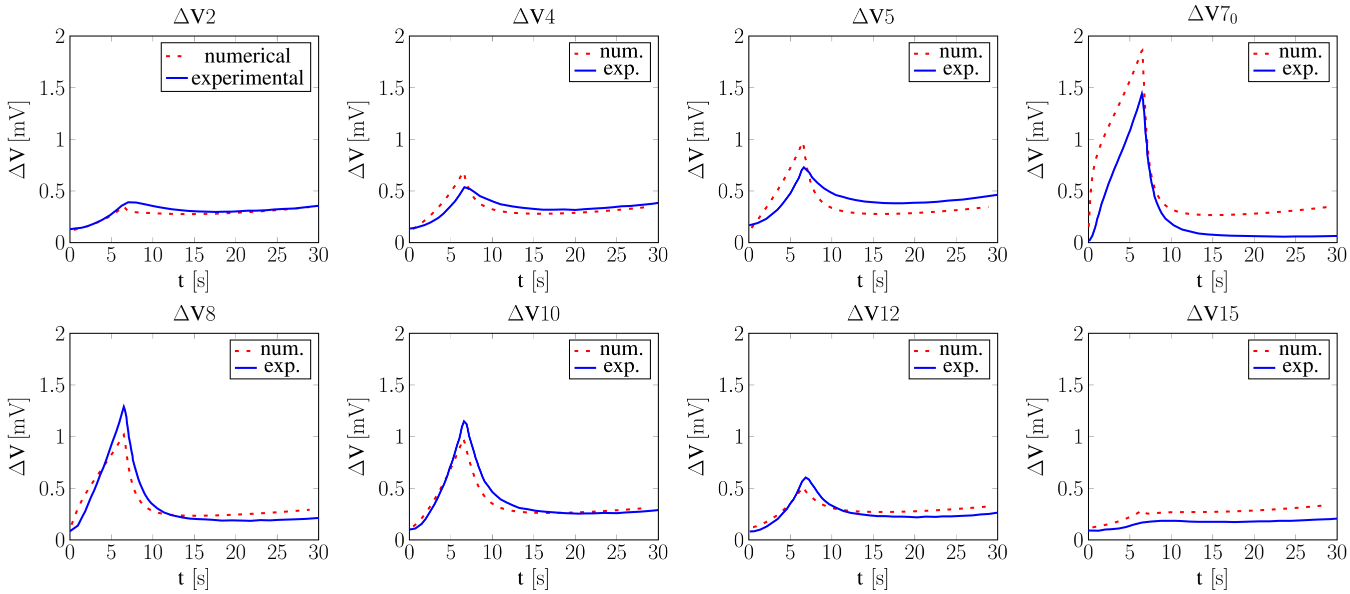

Fig. 4: Numerical and experimental voltage measurements at 66 K, 2 T background field and 700 A transport current.

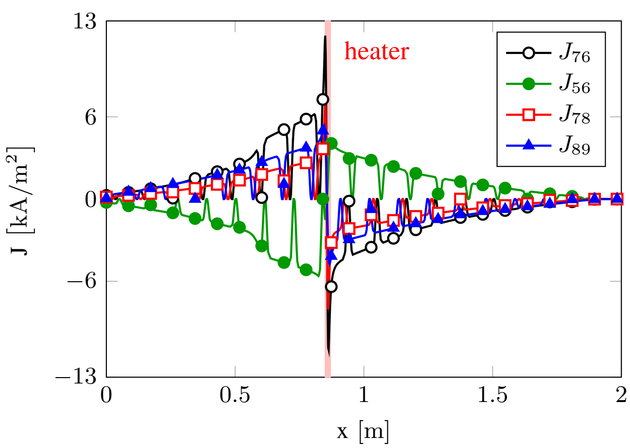

Fig. 5: Transversal current density (from the model) between strands #7-#6, #5-#6, #7-#8, #8-#9 at $t = 7.5$ s and working conditions of 66 K, 2 T, 700 A.

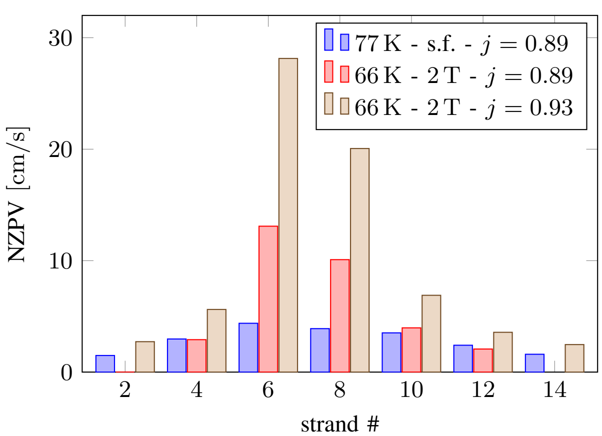

Fig. 6: Normal zone propagation velocities (from the model) for strands #2, #4, #6, #8, #10, #12, #14 at different working conditions.

strands nearer to strand #7 exhibit higher quench velocities. The velocity is computed at 77 K in self field with an transport current of 400 A corresponding to $j = 0.89$. These results can be compared with those found at working conditions of 66 K, 2 T by setting the current at 667 A corresponding to the same j value of 0.89. The NZPV for strand #6 increases from $4.4\,\mathrm{cm\,s^{-1}}$ at 77 K in self field to $13.1\,\mathrm{cm\,s^{-1}}$ at 66 K and 2 T. At 66 K, if j is set at 0.93, corresponding to a transport current of 700 A, the NZPV increases up to $28.1\,\mathrm{cm\,s^{-1}}$ for strand #6. A general remarkable increase of the quench propagation velocity is therefore observed at lower temperatures.

IV. Conclusion

An electro-thermal model developed for the analysis of quench in Roebel cable is applied here to study a pancake coil wound with Roebel cable. The model is validated by comparison with experimental results.

At 77 K in self field, the impact of the heater power on quench energy is analyzed: at heater powers above 0.8 W, the quench is adiabatic, with an energy of about 8 J - 9 J. At heater power values below 0.4 W, the heat and currents redistribute between strands and no quench occurs in the coil.

At 77 K in self field, the impact of the transport current on quench energy is also investigated. If the transport current is increased from 80 % to 99 % of critical current, the quench energy decreases by a factor 3.

The normal zone propagation velocity is computed at different working conditions. At 66 K and 2 T, the NZPV is up to 3 times higher than at 77 K and self field. At both working conditions, the coil is energized at 89 % of the critical current. The velocity further increases by a factor 2 if the transport current is increased at 93 % of the critical current.

References

[1] W. Goldacker, F. Grilli, E. Pardo, A. Kario, S. I. Schlachter and M. Vojeniak, "Roebel cables from REBCO coated conductors: a one-century-

old concept for the superconductivity of the future," *Supercond. Sci. Technol. 27 (2014) 093001 (16pp).*

[2] F. Grilli, "Numerical Modeling of HTS Applications," *IEEE Trans. Appl. Supercond., vol. 26, no. 3, pp. 1-8, April 2016.*

[3] D. C. van der Laan, J. D. Weiss, F. Scurti and J. Schwartz, "CORC wires containing integrated optical fibers for temperature and strain monitoring and voltage wires for reliable quench detection," *Supercond. Sci. Technol. 33 (2020) 085010 (22pp).*

[4] A. Zappatore, A. Augieri, R. Bonifetto, G. Celentano, L. Savoldi, A. Vannozzi, R. Zanino, "Modeling Quench Propagation in the ENEA HTS Cable-In-Conduit Conductor," *IEEE Trans. Appl. Supercond., vol. 30, no. 8, pp. 1-7, December 2020.*

[5] L. Rossi, A. Badel, M. Bajko, A. Ballarino, L. Bottura, M. M. J. Dhall, M. Durante, Ph. Fazilleau, J. Fleiter, W. Goldacker, E. Hr, A. Kario, G. Kirby, C. Lorin, J. van Nugteren, G. de Rijk, T. Salmi, C. Senatore, A. Stenvall, P. Tixador, A. Usoskin, G. Volpini, Y. Yang, N. Zangenberg, "The EuCARD-2 Future Magnets European Collaboration for Accelerator-Quality HTS Magnets," *IEEE Trans. Appl. Supercond., vol. 25, no. 3, pp. 7-7, June 2015.*

[6] G. A. Kirby, J. van Nugteren, A. Ballarino, L. Bottura, N. Chouika, S. Clement, V. Datskov, L. Fajardo, J. Fleiter, R. Gauthier, L. Gentini, L. Lambert, M. Lopes, J. C. Perez, G. de Rijk, A. Rijllart, L. Rossi, H. ten Kate, M. Durante, P. Fazilleau, C. Lorin, E. Hr, A. Stenvall, S. Caspi, M. Marchevsky, W. Goldacker, and A. Kario, "Accelerator-Quality HTS Dipole Magnet Demonstrator Designs for the EuCARD-2 5-T 40-mm Clear Aperture Magnet," *IEEE Trans. Appl. Supercond., vol. 25, no. 3, pp. 1-5, June 2015.*

[7] N.Glasson, M. Staines,R.Buckley,M. Pannu, and S.Kalsi, "Development of a 1 MVA 3-phase superconducting transformer using YBCO roebel cable," *IEEE Trans. Appl. Supercond., vol. 21, no. 3, pp. 13931396, June 2011.*

[8] P. Song, J. Zhu, T. Qu, P. Chen, F. Feng, and M. Qiu, "Design and test of a double pancake coil for SMES application wound by HTS Roebel cable," *IEEE Trans. Appl. Supercond., vol. 28, no. 4, pp. 15, June 2018.*

[9] V. Zermeno, F. Grilli1 and F. Sirois, "A full 3D time-dependent electromagnetic model for Roebel cables," *Supercond. Sci. Technol. 26 (2013) 052001 (8pp)*

[10] N. Amemiya, T. Tsukamoto1, M. Nii1, T. Komeda1, T. Nakamura1 Z. Jiang, "Alternating current loss characteristics of a Roebel cable consisting of coated conductors and a three-dimensional structure," *Supercond. Sci. Technol. 27 (2014) 035007 (16pp)*

[11] J. Ruuskanen, A. Stenvall, and V. Lahtinen, "Predicting Heat Propagation in Roebel-Cable-Based Accelerator Magnet Prototype: One-Dimensional Approach With Coupled Turns," *IEEE Trans. Appl. Supercond., vol. 27, no. 4, pp. 1-7, June 2017*

[12] S. Otten, A. Kario, E. Demencik, R. Nast and F. Grilli "Anisotropic monoblock model for computing AC loss in partially coupled Roebel cables," *Supercond. Sci. Technol. 33 094013*

[13] Y. Yang, J. Pelegrin, E. A. Young, R. Nast, A. Kario and W. Goldacker, "AC Losses of Roebel Cables with Striated 2G REBCO Strands," *IEEE Trans. Appl. Supercond., vol. 28, no. 4, pp. 1-5, June 2018*

[14] S. Otten, A. Kario, A. Kling and W. Goldacker, "Bending properties of different REBCO coated conductor tapes and Roebel cables at T = 77 K," *Supercond. Sci. Technol. 29 125003*

[15] J. van Nugteren, B. van Nugteren, P. Gao, L. Bottura, M. Dhall, W. Goldacker, A. Kario, H. ten Kate, G. Kirby, E. Krooshoop, G. de Rijk, L. Rossi, C. Senatore, S. Wessel, K. Yagotintsev, Y. Yang, "Measurement and Numerical Evaluation of AC Losses in a ReBCO Roebel Cable at 4.5 K," *IEEE Trans. Appl. Supercond., vol. 26, no. 3, pp. 1-7, April 2016*

[16] W. Pi, Z. Liu, S. Ma, Y. Meng, Q. Shi, J. Dong, Y. Wang, "Investigation on Thermal Stability of Quasi-Isotropic Superconducting Strand Stacked by 2 mm Wide REBCO Tapes and Cu Tapes," *IEEE Trans. Appl. Supercond., vol. 30, no. 4, pp. 1-6, June 2020.*

[17] P Gao, W A J Wessel, M Dhall, S Otten, A Kario, J Van Nugteren1, G Kirby, L Bottura and H. H. J. ten Kate, "Effect of resin impregnation on the transverse pressure dependence of the critical current in ReBCO Roebel cables," *Supercond. Sci. Technol. 32 (2019) 055006 (9pp)*

[18] L. Cavallucci, M. Breschi, P. L. Ribani, Q. Zhang and Y. Yang, "Electrothermal Modeling of Quench in REBCO Roebel Cables," *IEEE Trans. Appl. Supercond., vol. 28, no. 4, pp. 1-5, June 2018.*

[19] L. Cavallucci, M. Breschi, P. L. Ribani and Y. Yang, "Analysis of Current Distribution during Quench in a Pancake coil wound with REBCO Roebel cables," *presented at CHATS on Applied Superconductivity, Szczecin, Poland, July. 912, 2019*, available at https://indico.cern.ch/event/776034/contributions/3445062/attachments/1878595/3094376/CHATS_2019_final_Breschi.pdf

[20] Q. Zhang, Y. Yang, E. Young, L. Cavallucci, A. Kario, W. Goldacker, A. Usoskin, and L. Bottura, "Performance and Quench Characteristics of a Pancake Coil Wound with 2G YBCO Roebel Cable," *IEEE Trans. Appl. Supercond., vol. 28, no. 4, pp. 1-5, June 2018.*

[21] https://www.comsol.com

[22] LM. Kida, Y. Kikuchi, O. Takahashi and I. Michiyoshi "Pool-Boiling Heat Transfer in Liquid Nitrogen" *J. Nucl. Sci. Technology, vol. 28, no. 7, pp. 501-503 (1981)*

[23] M. Sumption, M. Majoros, C. Kovacs and E. W. Collings "Stability, quench and current sharing in Roebel and CORC cables for HEP magnets" *presented at the 13th European Conference on Applied Superconductivity EUCAS 2017, Geneva, Swiss, Sept. 1721, 2017*, available at https://kb.osu.edu/bitstream/handle/1811/88555/3Lo3-2-sumption-T-IV-rev.pdf?sequence=1&isAllowed=y

[24] L. Cavallucci, M. Breschi, P. L. Ribani, A. V. Gavrilin, H. W. Weijers and P. D. Noyes, "A Numerical Study of Quench in the NHMFL 32 T Magnet," *IEEE Trans. Appl. Supercond., vol. 29, no. 5, pp. 1-5, Augost 2019*

[25] M. Danial and J. Van Nugteren, "Parameterization of the critical surface of REBCO conductors from Bruker," *CERN STUDENTS Note 017 013 CERN*, available at: https://cds.cern.ch/record/2277484/files/Bruker%20HTS%20Fit.pdf

[26] I. Falorio, E. A. Young and Y. Yang, "Quench Characteristic and Minimum Quench Energy of 2G YBCO Tapes," *IEEE Trans. Appl. Supercond., vol. 25, no. 3, pp. 1-5, June 2015.*

[27] J.van Nugteren, M.Dhall, S.Wessel, E.Krooshoop, A.Nijhuis H.ten Kate, "Measurement and analysis of normal zone propagation in a ReBCO-coated conductor at temperatures below 50 K," *Physics Procedia, vol. 67, pp. 945-951, 2015.*